International Journal of Design & Nature and Ecodynamics
Vol. 20, No. 7, July, 2025, pp. 1615-1624
Journal homepage: http://iieta.org/journals/ijdne

Dose-Dependent in Vivo Toxicity and Structural Evaluation of MgO Nanoparticles Synthesized via Pulsed Laser Ablation in Liquid

Ruwaida A. Sami[1*], Wisam J. Aziz[1], Khetam Habeeb Rasool[2]

[1] Department of Physics, College of Science, Mustansiriyah University, Baghdad 10052, Iraq
[2] Department of Biology, College of Science, Mustansiriyah University, Baghdad 10052, Iraq

Corresponding Author Email: ruwaida.arif@uomustansiriyah.edu.iq

Copyright: ©2025 The authors. This article is published by IIETA and is licensed under the CC BY 4.0 license (http://creativecommons.org/licenses/by/4.0/).

https://doi.org/10.18280/ijdne.200718

Received: 22 June 2025
Revised: 21 July 2025
Accepted: 26 July 2025
Available online: 31 July 2025

Keywords:
MgO NPs, pulsed laser ablation in liquid (PLAL), MgO NPs dose toxicity, histopathological effects

ABSTRACT

This work details the synthesis, comprehensive characterization, and in vivo toxicity assessment of magnesium oxide nanoparticles (MgO NPs) produced by pulsed laser ablation in liquid. A high-purity magnesium sheet (99.99%) was subjected to 400 laser pulses using a Nd:YAG laser system (1064 nm wavelength, 900 mJ pulse energy, 8 Hz frequency) in 4 mL deionized water. Subsequently, the synthesized nanoparticles were characterized using multiple analytical techniques. X-ray diffraction confirmed cubic-phase MgO, showing an average crystal size of 10 nm. TEM indicated cubic-shaped particles with an average diameter of 11 nm, while scanning electron microscopy showed agglomerated structures with individual particle sizes of 17.6 nm. Furthermore, UV-visible spectroscopy demonstrated a direct band gap of 5.9 eV with an absorption peak at 200 nm. In vivo toxicity evaluation was conducted using male albino rats exposed to different concentrations (100, 150, and 200 mg L^{-1}) for 28 days. Results demonstrated dose-dependent toxicity with significant hematological changes, including increased white blood cell counts and decreased mean corpuscular hemoglobin. Additionally, histopathological examination revealed progressive liver damage ranging from mild vacuolar degeneration at 100 mg L^{-1} to severe necrosis at 200 mg L^{-1}, along with kidney damage including glomerular hypercellularity and tubular swelling. These findings indicate that concentrations exceeding 100 mg L^{-1} cause toxicity changes, necessitating careful dose regulation for potential biomedical and environmental applications.

1. INTRODUCTION

The field of nontechnology has revolutionized various scientific trends through its ability to modify materials at the nano scale (1-100 nm) [1, 2]. Nanomaterials exhibit superior mechanical strength, enhanced chemical reactivity, and unique optical properties compared to their bulk counterparts. These exceptional characteristics arise from their small-scale dimensions and increased surface area to volume ratio [2, 3]. Consequently, these properties have enabled widespread applications across medicine, electronics, environmental research, and energy storage sectors [4, 5].

In biomedical research, nanotechnology has boosted multiple therapeutic approaches. It has improved targeted drug delivery systems, improved diagnostic imaging capability, and improved the effectiveness of healing treatments [6, 7]. However, the increasing prevalence of nanoparticles has raised critical concerns regarding toxicity and environmental impact. Therefore, understanding nanoparticle-biological interactions has become essential for ensuring safe application and obtaining regulatory approval [8, 9]. Within the category of metal oxide nanomaterials, MgO NPs have attracted considerable scientific interest due to their versatile applications. These nanoparticles demonstrate broad utility in food preservation systems, drug delivery mechanisms, and catalytic processes [10, 11].

In biomedical contexts, MgO NPs have been extensively investigated for their potent antibacterial properties and wound healing enhancement capabilities. Additionally, they show significant potential as drug delivery carriers [12, 13]. Recent studies have demonstrated promising applications in cancer treatment, where they can induce cancer cell death while preserving healthy tissues.

Recent research has revealed promising applications in cancer therapeutics, where MgO nanoparticles can selectively induce cancer cell death while preserving healthy tissue integrity [14, 15]. Nevertheless, concerns persist regarding their potential toxicity, particularly related to bioaccumulation in vital organs during prolonged exposure periods [16-18].

The synthesis of magnesium oxide nanoparticles employs various methodological approaches. These methods include chemical synthesis routes, sol-gel processing techniques, and plasma-assisted methods [19]. Among these methods, pulsed laser ablation in liquid (PLAL) provides several advantages over traditional synthesis methods. This technique offers an eco-friendly approach that requires no toxic solvents. Additionally, it eliminates the need for reducing agents, representing a chemical-free synthesis route. Moreover, PLAL

enables precise control over particle properties through adjustable laser parameters. Furthermore, the technique produces high-purity NPs without chemical contamination. Consequently, the final products maintain excellent purity levels. PLAL also allows rapid synthesis with minimal processing steps. The technique creates NPs with unique surface properties due to the high-energy laser process. Therefore, these particles exhibit enhanced reactivity resulting from the laser-induced formation mechanism [20, 21].

MgO NPs synthesized via PLAL have displayed excellent optical features [20, 21]. Furthermore, PLAL-produced MgO nanoparticles exhibit superior antibacterial activity, showing effectiveness against pathogenic bacteria including E. coli and Staphylococcus aureus [22, 23]. These nanoparticles show potential for biosensor and drug delivery applications due to their biocompatibility and unique surface characteristics [24].

However, these synthesis methods have proven effective. Nevertheless, concerns exist regarding MgO NP in vivo toxicity. In vitro studies have evaluated effects on various cell types. Specifically, liver, kidney, and lung cells were examined. These studies revealed dose-dependent cytotoxic effects. Furthermore, higher concentrations result in significant cell viability reduction [25, 26]. Similarly, in vivo studies, particularly using mouse models, have demonstrated dose-dependent toxicity manifesting as histological changes in critical organs, including the kidneys and liver. For instance, high doses of MgO NPs have been shown to cause liver damage characterized by bile ductule proliferation and hepatic sinusoid congestion [27, 28].

To the best of our knowledge, based on an extensive literature review, no previous studies have reported the synthesis of MgO nanoparticles from high-purity magnesium sheets using pulsed laser ablation in deionized water. While previous research has investigated the toxicity of MgO NPs synthesized through other methods, the in vivo toxicity profile of MgO NPs produced through this eco-friendly, chemical-free approach remains unexplored. Therefore, the present study's novelty lies in investigating the in vivo toxicity of these uniquely synthesized MgO NPs through comprehensive hematological and histopathological analyses in albino male rats. This research provides critical insights into their safety profile for potential biomedical applications.

2. MATERIALS AND METHODS

2.1 Synthesis MgO NPs

The experimental setup consisted of an Nd: YAG laser system known for its effectiveness in high-energy applications. The system is set to produce a laser beam with an energy output of 900 millijoules. It was operating at a frequency of 8 Hz and a wavelength of 1064 nm, and a 6 ns pulse duration with a 250 mm focal length lens to produce a spot size of 5.51 mm^2, making it suitable for inducing the necessary reactions for nanoparticle synthesis. These settings were utilized to optimize practical size and maintain process stability [29]. High-purity magnesium sheet (99.99% purity, Batch No. 652247/470611) was obtained from British Drug Houses Ltd., London.

The sheet was immersed in a glass beaker containing 4 mL of deionized water at room temperature (with a pH around 7), providing a suitable liquid environment to facilitate the laser ablation process. It was subjected to a series of 400 laser pulses, effectively striking the material and facilitating the formation of magnesium oxide nanoparticles. Following the synthesis, the atomic concentration of MgO nanoparticles dispersed in water was determined using atomic absorption spectroscopy (AAS). Based on the calibration curve for magnesium, the measured concentration was 200 mg L^{-1}.

Comprehensive characterization employed multiple analytical techniques to evaluate the synthesized nanoparticles. X-ray diffraction (XRD) analysis utilized an Xpert Panalytical Phillips system (Netherlands) for crystalline structure identification. Scanning electron microscopy (SEM) was performed using a MIRA3 TESCAN system to examine surface morphology.

Additionally, transmission electron microscopy (TEM) employed a JEM-ARM200F instrument for nanoscale particle size and shape analysis. These complementary characterization methods provided a thorough evaluation of the nanoparticles' structural and morphological properties.

2.2 Animals model

Albino male rats at eight weeks old, healthy and weighing between 140–190 g, were selected. They were obtained from the University of Al-Nahrain. They came from the Biotechnology Research Center's Animal House. The animals were housed in plastic cages within air-conditioned rooms. A 12-hour light/dark cycle was maintained. The room temperature was kept between 22-24℃ (±2℃). Access to food and water remained unrestricted. Sixteen rats were weighed and divided into four groups. Each group consisted of four rats with closed weights. The first group was considered the control, while the rest were as test groups. The experiment started after one week of acclimation when the animal age at nine weeks old. They received MgO NPs at different dosages. The rats in the control group were kept untreated, while the rest were administered various dosages of the prepared solution orally to test its toxicity. The animals in groups 2-4 received 0.5 mL daily based on their weights of MgO containing dosages of (100 mg L^{-1}, 150 mg L^{-1}, and 200 mg L^{-1}), respectively. The animals' weights were observed throughout the experiment period by measuring their weight each week. After 30 days, the trial was over, and the animals were euthanized to check the toxicity using histological and hematological examinations. All animal procedures followed the guidelines of the Institute for Laboratory Animal Research. They also complied with the Animal Research: Reporting of In Vivo Experiments (ARRIVE) guidelines [30].

2.3 Blood samples analysis

The animals were anesthetized to enable proper handling procedures. Isoflurane served as the anesthetic agent. Piramal Enterprises Limited (Telangana, India) produced this compound. Immediately following anesthesia, blood samples were collected using sterile syringes. The samples were then transferred into EDTA-coated tubes to prevent coagulation and processed promptly for hematological analysis.

A complete blood count was performed using an automated hematology analyzer for each collected sample. This assessed the potential systemic effects of MgO NPs.

The hematological parameters measured included red blood cells (RBCs), white blood cells (WBCs), hemoglobin (Hb) levels, hematocrit (HCT), mean corpuscular volume (MCV), mean corpuscular hemoglobin (MCH), and mean corpuscular

hemoglobin concentration (MCHC).

2.4 Histological analysis

Histological examination was conducted for renal and hepatic tissues to explore morphological alterations caused by the MgO NPs. Orgain specimens were cleaned with deionized water to remove blood initially. Then, the specimens were placed in 10% formalin solution and embedded in paraffin blocks. Also, they sectioned into 5 µm thick slices by using a microtome.

The tissue sections were then processed for Hematoxylin and Eosin (H&E) staining. In addition, they were deparaffinized, rehydrated through graded alcohols, and stained with hematoxylin for nuclear visualization, followed by eosin counterstaining for cytoplasmic detail.

The stained sections were examined under a light microscope at different magnifications (40×, 100×, and 400×). representative photomicrographs were captured for documentation and analysis.

2.5 Statistical analysis

Data analysis was employed using GraphPad Prism software version 10. Analysis of variance (ANOVA) was conducted initially. Dunnett's multiple comparisons test followed the ANOVA test [31]. Statistical significance was determined using $P \leq 0.05$. Mean differences meeting this criterion were considered significant. Data are expressed as mean ± standard deviation. Each experimental group contained four subjects (n = 4).

3. RESULTS AND DISCUSSION

3.1 Structural analysis

XRD analysis was used to identify the phases in the MgO NPs. It assessed the crystal size, purity, and crystallinity of particles produced by pulsed laser ablation. Diffraction angles (2θ) were compared with literature data (JCPDS card No.). Figure 1 shows the XRD refinement pattern for angles from 20° to 70°.

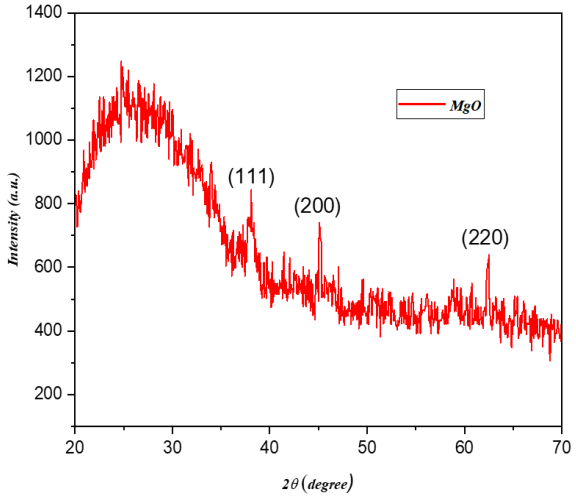

Figure 1. XRD pattern of MgO NPs synthesis by pulsed laser ablation in liquid

From Figure 1, it can be observed that three peaks are distinguished when 2θ is equivalent to 38, 45, and 62. These angles conform to 111, 200, and 220 planes, respectively, which refer to cubic MgO NPs (PDF- 00-004-0829). The Full Width at Half Maximum (FWHM) was estimated for the peaks observed in the XRD test, and the Debye-Scherrer formula [32], given by Eq. (1), was utilized to calculate crystal size.

$$D = \frac{0.9\lambda}{\beta \cos\theta} \quad (1)$$

where, D is referred to as the average crystal size, while λ represents the x-ray wavelength and in this case is equal to 1.504 nm and β is FWHM. The study found that the average crystal size of MgO NPs was 10 nm.

3.2 UV-Visible spectroscopy

The MgO NPs were tested in the UV spectrophotometer to detect their UV-visible spectra. The wavelength range between 200-1200 nm was examined to determine the absorbance of MgO NPs. The absorption peak of MgO NPs at 200 nm is presented in Figure 2.

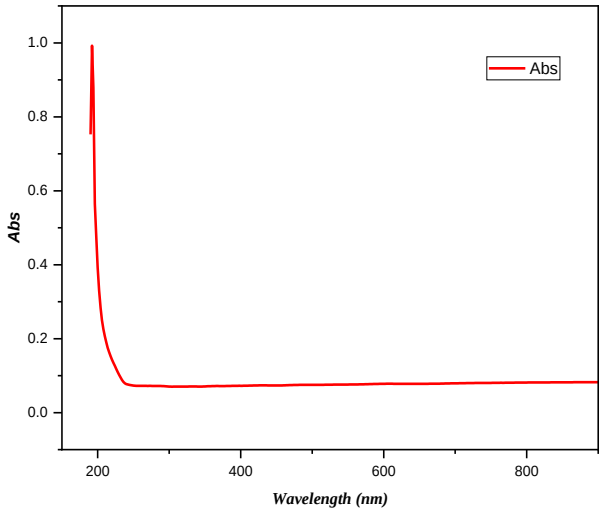

Figure 2. UV absorption spectrum of MgO NPs

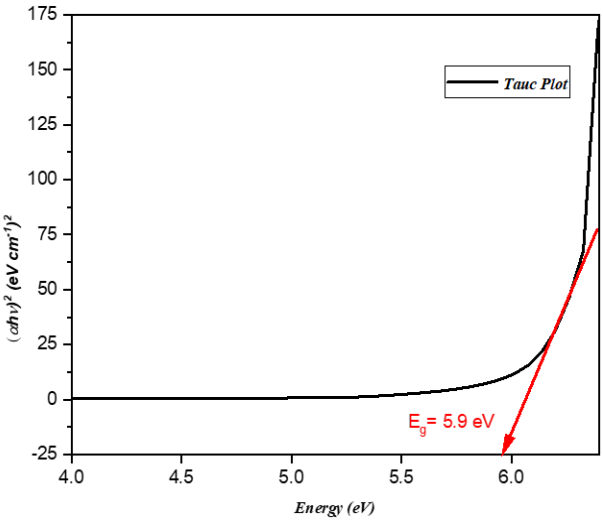

Figure 3. Optical band gap energy of MgO NPs

The energy band gap of the prepared MgO NPs was calculated by using Tauc's equation as shown in Eq. (2) [33]:

$$(\alpha h\nu) = A\,(h\nu - Eg)^{n} \quad (2)$$

where, A is a constant and α is the absorption coefficient, while h represents Planck's constant. Eg refers to the energy band gap, while (n = ½) for the direct band gap. MgO NPs band gap was estimated by extrapolating the curve plotted between energy (eV) and $(\alpha h\nu)^2$, as shown in Figure 3. The energy band gap was calculated by extrapolating the curve, estimated value of 5.9 eV. These findings agree with the previous study that investigated the same material [34].

3.3 Transmission electron microscopy (TEM) analysis

TEM test was done to study the size, shape, and clustering of the MgO nanoparticles. The TEM image in Figure 4(a) showed that the MgO nanoparticles had a cubic shape. However, the particles were heavily clustered together. As a result, they formed larger groups with unclear shapes. Despite this clustering, individual particles still showed cubic features where they could be seen clearly. Particle size was measured using ImageJ software [35]. The results showed that the average diameter was 11 nm. This information is displayed in the size distribution chart in Figure 4(b). Furthermore, the clustering behavior is normal for MgO nanoparticles. This happens because they have high surface energy.

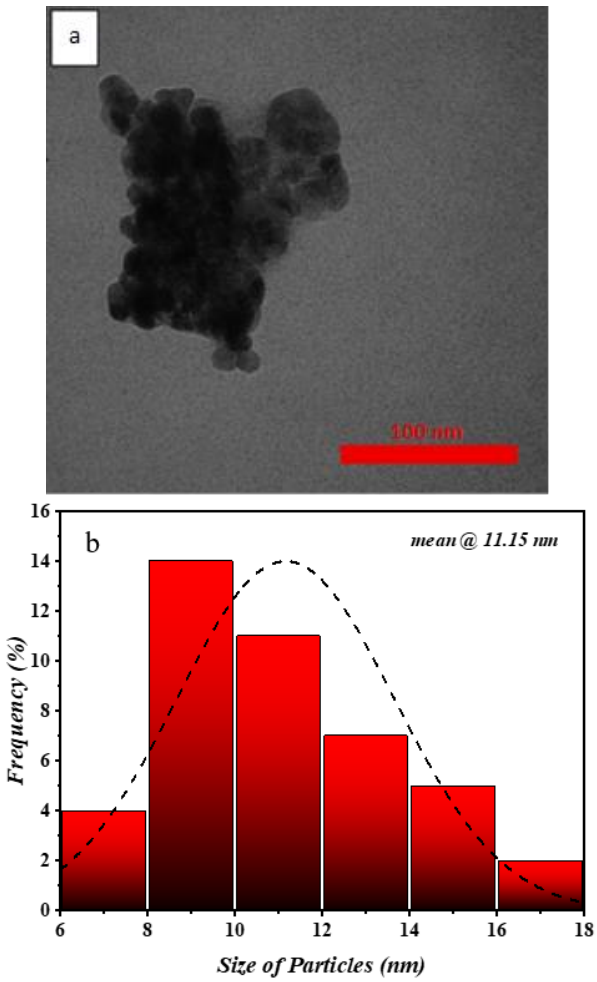

Figure 4. (a) TEM image with 100 nm scale of MgO NPs (b) Histogram of size distribution

3.4 Scanning electron microscopy (SEM) analysis

SEM images in Figure 5 were used to evaluate the morphology of the MgO NPs produced via PLAL. The SEM analysis revealed that the nanoparticles formed large agglomerates rather than individual cubic structures. At higher magnifications, the particles showed a sheet-like morphology. Moreover, these particles were fused and heavily aggregated together. The large aggregates displayed elongated, spine-like forms, as clearly visible in the images. Furthermore, the nanoparticles were strongly attached to each other and could not be separated easily. Figure 5 shows that the diameter of the MgO NPs synthesized by the PLAL method is 17.6 nm. However, this measurement reflects individual particle size within the larger structures. The formation of these large agglomerates can be explained by the high surface energy of MgO NPs. Additionally, the increased surface area to volume ratio creates strong attractive forces. As a result, the nanoparticles cluster together to form these complex morphologies [36]. This aggregation behavior affects both the sheet-like appearance and the spine-like structures observed in the SEM images. In addition, such behavior may influence the NPs' bioactivity as a larger cluster could reduce cellular uptake and bioavailability compared to individual particles.

The SEM measurement represents surface features or particle aggregates. Conversely, the TEM measurement of 11 nm reflects individual particle size more accurately. This occurs because TEM offers better resolution than SEM [37]. Therefore, TEM can distinguish individual particles within clusters, while SEM visualizes them as larger, single objects.

3.5 Animals' observation

During the experiment period, each rat was examined twice daily, and no deaths were recorded. There was a statistical variation in the mean body weights of groups that were treated with different dosages of MgO NPs (100 mg L^{-1}, 150 mg L^{-1}, and 200 mg L^{-1}) compared to the control group ($P < 0.01$), as presented in Figure 6. These findings confirm that the growth retardation of the animals can be related to accumulated MgO NPs in the liver and kidneys, leading to toxicity. This accumulation can ruin organ function, which may contribute to weight loss [25, 38].

3.6 Hematology analysis

Following the 30-day oral exposure of MgO NPs at different concentrations, the hematological parameters were examined. Hematological profiles can be utilized to diagnose the level of a foreign compound's detrimental impact on an animal's blood components [39, 40]. Table 1 presents the concentration-dependent hematology outcomes of the MgO NPs, which show that the WBC levels were elevated at a 150 mg L^{-1} dose ($P < 0.05$) and increased at a 200 mg L^{-1} dose ($P < 0.01$). This can be due to an increase in organ infection and inflammation. These outcomes agree with the findings in study [41]. The elevated WBC count may result from oxidative stress-mediated immune activation rather than classical inflammatory pathways. MgO nanoparticles can induce direct oxidative damage to immune cells, triggering compensatory white blood cell proliferation [42]. On the other hand, the MCH levels were affected at both mg L^{-1} ($P < 0.05$) and 200 mg L^{-1} doses ($P < 0.01$), which is due to changes in cellular physiology that lead to abnormal oxygenation from the lungs

and reduced oxygen in the bloodstream [11, 43]. No impact was noted in hematologic parameters in comparison to the control groups. Figure 7 shows a bar graph of mean ± SD of hematological parameters compared to the control group, with other groups treated with various MgO NPs.

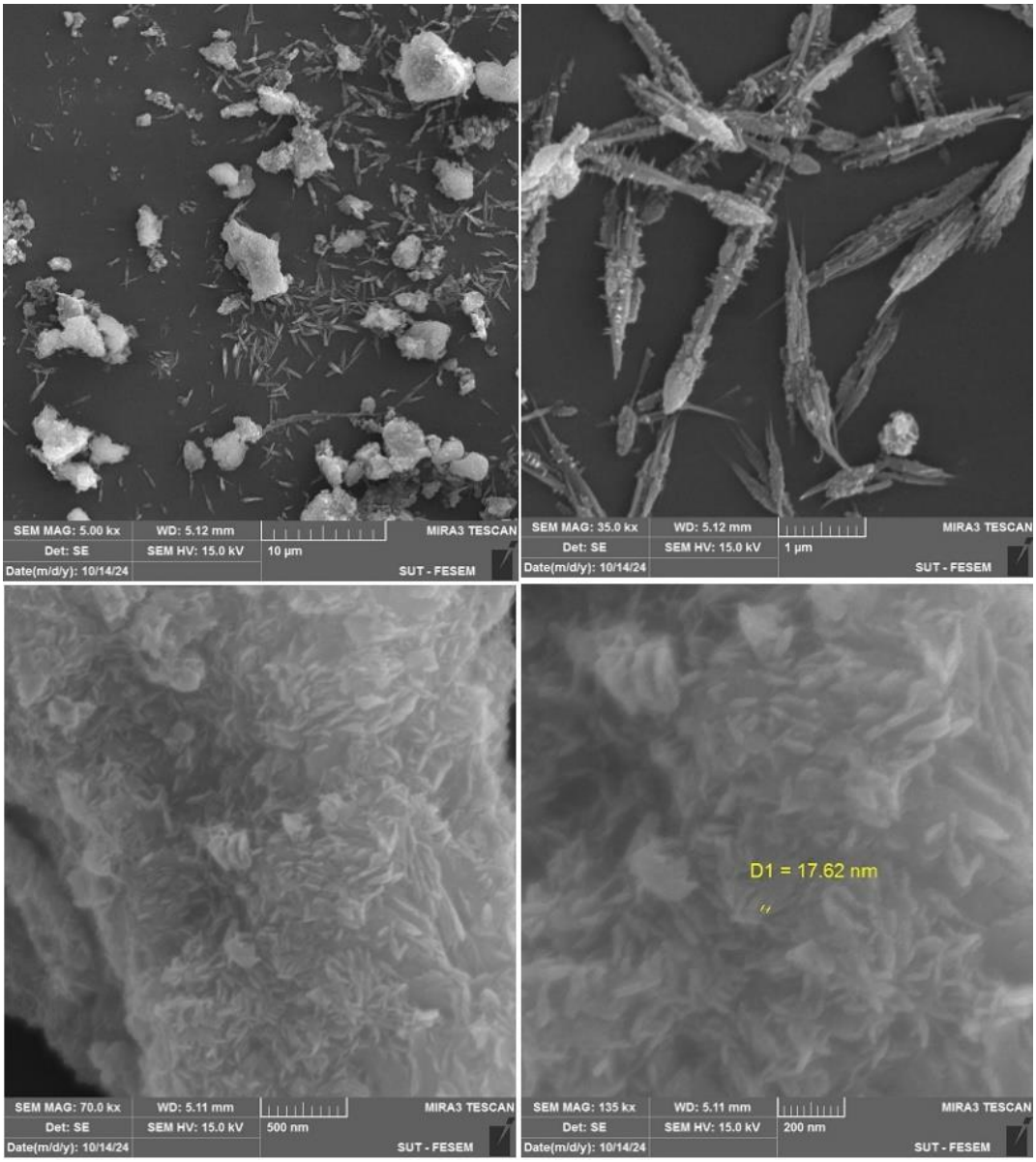

Figure 5. SEM image of MgO NP synthesis by pulsed laser ablation method at different scales

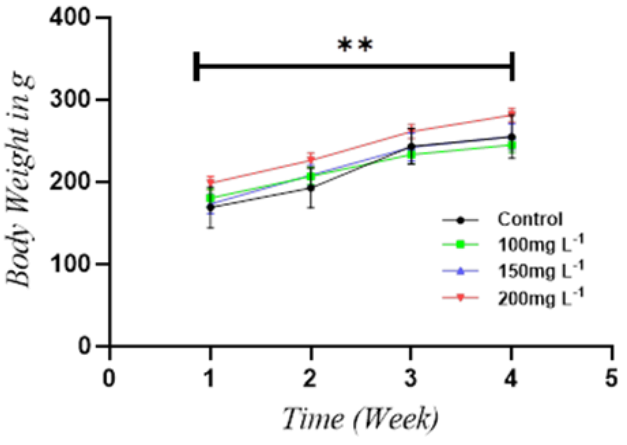

Figure 6. Rats' mean body weight after orally receiving MgO NPs at the doses of 100, 150, and 200 mg L^{-1} for 30 days
Data are presented as mean ± SD (n = 4). (** refer to P < 0.01 vs. control).

3.7 Liver sections histopathological analysis

Histopathological examination of liver samples showed dose-dependent liver damage from MgO NPs (Figure 8). Control group animals had normal liver structure with healthy central veins, liver cords, portal areas, liver units, blood spaces, immune cells, and liver cells (Figure 8(a)). Administration of 100 mg L^{-1} MgO NPs caused mild liver changes. These included slight blocking of central veins and small empty spaces in liver cells (Figure 8(b)). However, at a 150 mg L^{-1} dose, more serious changes occurred. Specifically, immune cells entered the liver tissue, and liver cells developed mild empty spaces in their interior (Figure 8(c)). The highest dose (200 mg L^{-1}) caused severe liver damage. This included heavy blocking of central veins and large empty spaces in liver cells. Furthermore, liver cell death occurred along with immune cell clusters in the liver tissue (Figures 8(d-e)), and a mild immune cell invasion was found in the portal areas (Figure 8(f)).

3.8 Kidney sections histopathological analysis

Kidney examination showed dose-related damage from MgO NPs (Figure 9). Control group rats had normal kidney structure with a healthy outer layer and inner region, including normal filtering units and kidney tubes (Figure 9(a)). However, administration of 100 mg L^{-1} MgO NPs caused changes in the filtering units. Specifically, too many cells grew in the filtering clusters, and the surrounding space disappeared (Figure 9(b)). Furthermore, at a 150 mg L^{-1} dose, damage became worse as filtering clusters had severe cell overgrowth. Additionally, kidney tube cells swelled up, which narrowed and blocked their openings (Figure 9(c)). Moreover, the highest dose (200 mg L^{-1}) caused severe damage with extreme cell overgrowth in filtering clusters. In addition, kidney tube cells developed serious granular changes in their interior (Figure 9(d)).

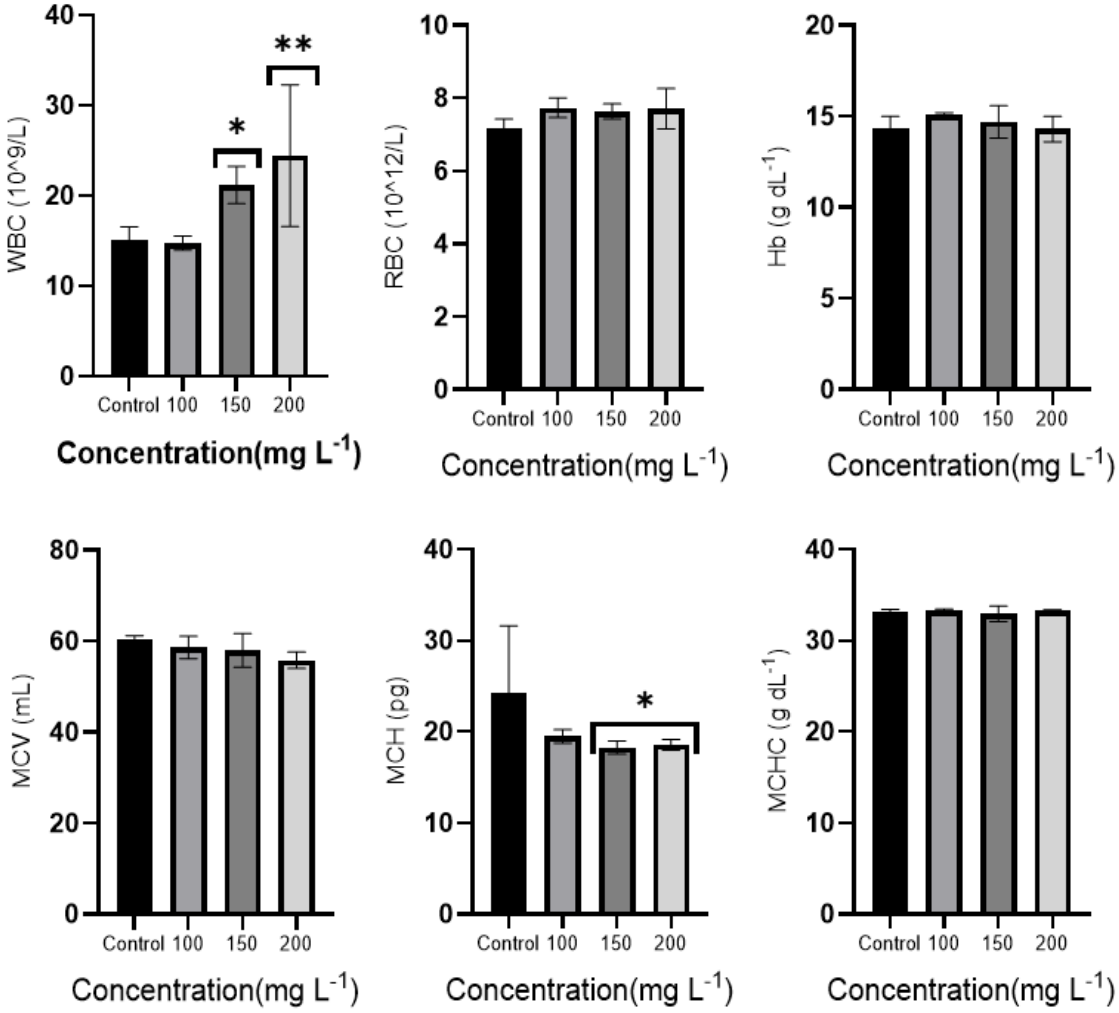

Figure 7. The results of hematological analysis for male rats administered with MgO NPs after 30 days at various doses (100, 150, and 200 mg L^{-1})

Values are means ± SD (n = 4) (* refer to P < 0.05 and ** refer to P < 0.01, in contrast to the control group).

Table 1. The hematological parameters (Mean ± SD) of animals exposed to different doses of MgO NPs

Parameter	Control	100 mg L^{-1} Mean ± SD	150 mg L^{-1} Mean ± SD	200 mg L^{-1} Mean ± SD
WBC (10^9/L)	15.1 ± 1.44	14.76 ± 0.80	21.19 ± 2.08*	24.44 ± 7.85**
RBC (10^{12}/L)	7.16 ± 0.27	7.74 ± 0.27	7.64 ± 0.21	7.72 ± 0.56
Hb (g dL^{-1})	14.3 ± 0.70	15.10 ± 0.10	14.70 ± 0.89	14.30 ± 0.70
MCV (mL)	60.33 ± 0.93	58.63 ± 2.47	58.00 ± 3.73	56.50 ± 1.85
MCH (pg)	24.30 ± 7.36	19.50 ± 0.75	18.27 ± 0.70*	18.57 ± 0.58*
MCHC (g dL^{-1})	33.10 ± 0.36	33.33 ± 0.15	32.97 ± 0.85	33.27 ± 0.15

Data are expressed as mean ± SD (n = 4 per group). *P < 0.05 and **P < 0.01 vs. control group

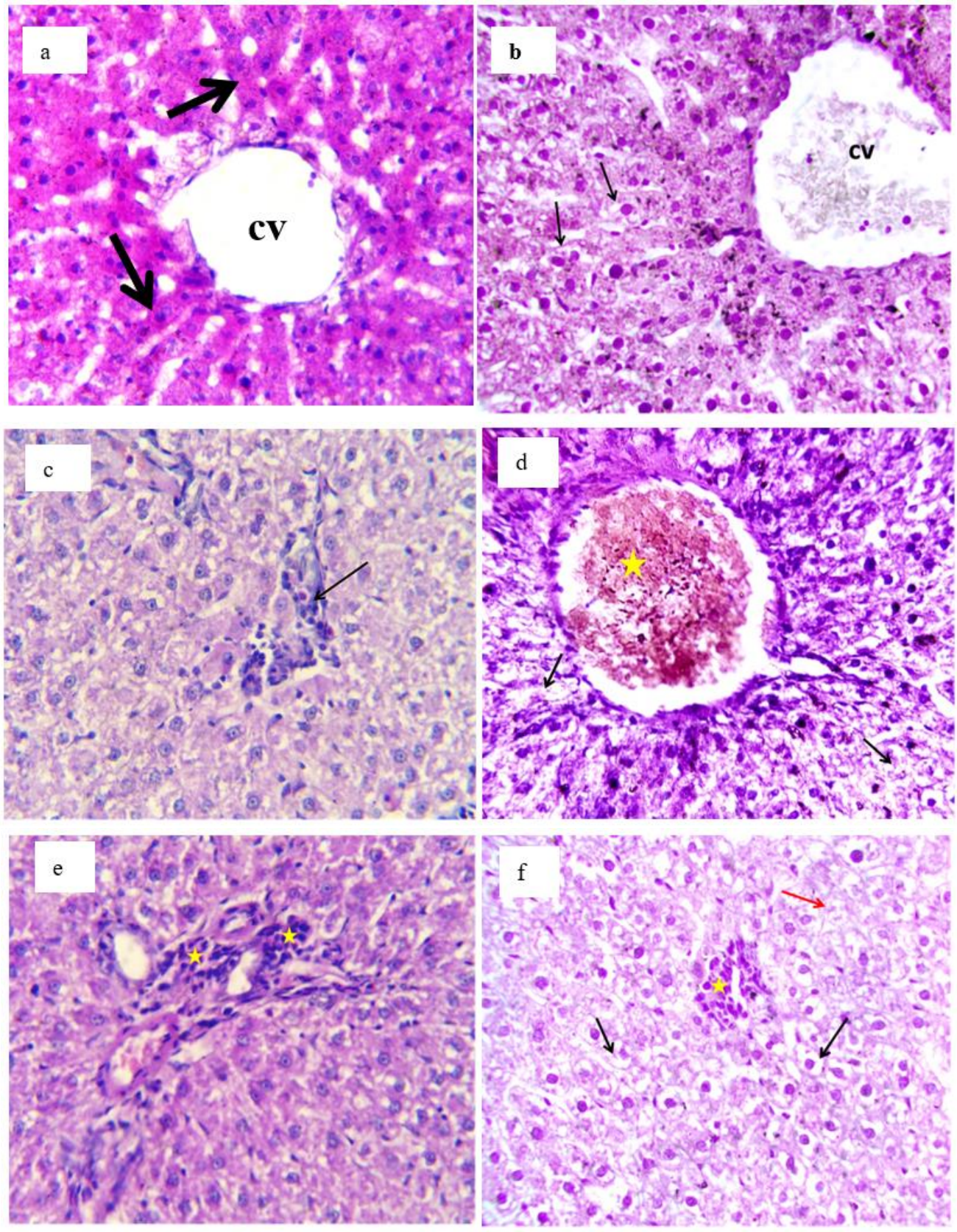

Figure 8. Histopathological examination of rat liver tissue following MgO NPs exposure (H&E stain, ×400). (a) Control group showing normal hepatic architecture, (b) 100 mg/L MgO NPs treatment, (c) 150 mg/L MgO NPs treatment, (d-f) 200 mg/L MgO NPs treatment showing various hepatic lesions

cv: Central vein; arrows indicate specific pathological features; asterisks mark areas of concern.

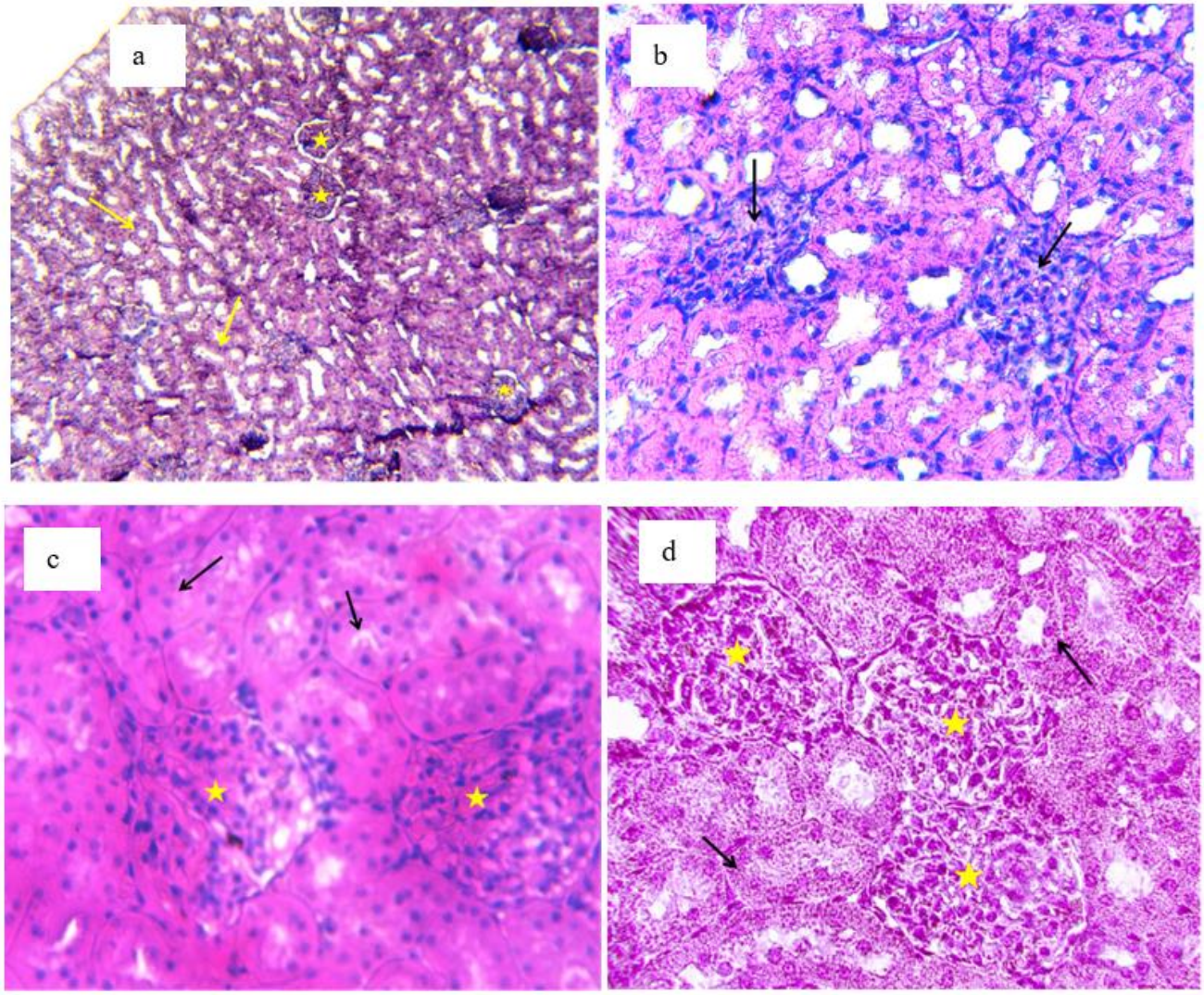

Figure 9. Kidney tissue sections from rats treated with MgO NPs (H&E stain). (a) Control group (×100), (b) 100 mg L^{-1} dose (×400), (c) 150 mg L^{-1} dose (×400), (d) 200 mg L^{-1} dose (×400)
Arrows and asterisks indicate specific features.

4. CONCLUSIONS

This study successfully synthesized MgO NPs at 900 mJ laser beam energy using pulsed laser ablation in liquid (PLAL) method. The synthesis was achieved through an Nd:YAG laser system operating at 8 Hz frequency and 1064 nm wavelength. The XRD analysis confirmed the cubic shape of the produced MgO NPs, while the UV-Vis spectroscopy showed a wide band gap of 5.9 eV. Further, TEM and SEM analyses indicate the nanoscale dimensions and morphology of the synthesized particles, which may improve their reactivity and surface interactions.

The toxicity assessment showed dose-dependent effects in male albino rats and hematological changes (increased WBC level and hematological alterations). Also, the histopathological examination revealed damage to the liver and kidneys. These findings bring attention to the importance of cautious dosage regulation for MgO NPs in biomedical or environmental applications, particularly at concentrations exceeding 100 mg L^{-1}.

While pulsed laser ablation in liquid (PLAL) is a promising method for synthesizing MgO NPs, our findings highlight the need for careful toxicity profiling before they can be used safely. To move these particles toward medical and industrial uses, future studies should focus on practical strategies to reduce their biological risks. This includes modifying their surface with biocompatible coatings and optimizing the synthesis process to better control particle size and shape, such as reducing the beam energy. These steps are essential for ensuring the safe and effective use of MgO NPs.

ACKNOWLEDGEMENTS

The authors would like to thank Mustansiriyah University (www.uomustansiriyah.edu.iq), Baghdad, Iraq, for its support in this work.

REFERENCES

[1] Trotta, F., Mele, A. (2019). Nanosponges: Synthesis and Applications. John Wiley & Sons. https://doi.org/10.1002/9783527341009
[2] Sharma, P.K., Dorlikar, S., Rawat, P., Malik, V., Vats, N., Sharma, M., Rhyee, J.S., Kaushik, A.K. (2021).

Nanotechnology and its application: A review. Nanotechnology in Cancer Management, 1-33. https://doi.org/10.1016/B978-0-12-818154-6.00010-X

[3] Khalid, A., Jaber, G.S., Dhaif, S.S. (2023). Preparation of TiO_2NPs by laser and study its antibacterial activity against bacterial pathogens. AIP Conference Proceedings, 2977(1): 040055. https://doi.org/10.1063/5.0183601

[4] Raheema, M.H., Jaber, G.S. (2023). Synthesis of carbon nanotubes using modified hummers method for cathode electrodes in dye-sensitized solar cell. Baghdad Science Journal, 20(6). https://doi.org/10.21123/bsj.2023.7150

[5] Ahmed, R.S., Dahham, A.M., Abdalameer, N.Kh., Mohammed, R.S. (2025). Optical, structural and biological properties of reduced silver oxide nanoparticles from *Anethum Graveolens* leaf extract by nonthermal plasma. Nano LIFE, 15(5): 2450025. https://doi.org/10.1142/S1793984424500259

[6] Oberdörster, G., Oberdörster, E., Oberdörster, J. (2005). Nanotoxicology: An emerging discipline evolving from studies of ultrafine particles. Environmental Health Perspectives, 113(7): 823-839. https://doi.org/10.1289/ehp.7339

[7] Talib, W.R., Sudhakaran, A., Sudhakaran, A., Mohammed, R.S. (2024). Potential biological and optoelectronic applications of AgO: ZnO nanocomposite synthesized by green approach. The European Physical Journal Plus, 139(12): 1118. https://doi.org/10.1140/epjp/s13360-024-05920-7

[8] Jaber, G.S., Dhaif, S.S., Hussian, T.A.A., Ibrahim, N.A., Arifiyanto, A. (2023). Enhancing the prodigiosin pigment by adding Ag\TiO_2 synergism for antibacterial activity. Biocatalysis and Agricultural Biotechnology, 54: 102900. https://doi.org/10.1016/j.bcab.2023.102900

[9] Nagchowdhury, P., Krishna, M., Patra, C.R. (2024). Biomedical applications of magnesium oxide nanoparticles. In Nanomaterials for Biomedical and Bioengineering Applications, pp. 97-132. https://doi.org/10.1007/978-981-97-0221-3_5

[10] Gatou, M.A., Skylla, E., Dourou, P., Pippa, N., Gazouli, M., Lagopati, N., Pavlatou, E.A. (2024). Magnesium oxide (MgO) nanoparticles: synthetic strategies and biomedical applications. Crystals, 14(3): 215. https://doi.org/10.3390/cryst14030215

[11] Mohammed, R.S., Aadim, K.A., Ahmed, K.A. (2022). Estimation of in vivo toxicity of MgO/ZnO core/shell nanoparticles synthesized by eco-friendly non-thermal plasma technology. Applied Nanoscience, 12(12): 3783-3795. https://doi.org/10.1007/s13204-022-02608-1

[12] Nguyen, N.Y.T., Grelling, N., Wetteland, C.L., Rosario, R., Liu, H. (2018). Antimicrobial activities and mechanisms of magnesium oxide nanoparticles (nMgO) against pathogenic bacteria, yeasts, and biofilms. Scientific Reports, 8(1): 16260. https://doi.org/10.1038/s41598-018-34567-5

[13] Mohamad, E.A., Gad, A.M., Abd El-Rhman, R.H., Moselhey, M.T., Madian, N.G. (2024). Dressing membrane composites of PVA/chitosan/MgO nanoparticles for wound healing applications in rat model. Naunyn-Schmiedeberg's Archives of Pharmacology, 398: 6989-7003. https://doi.org/10.1007/s00210-024-03716-1

[14] Di, D.R., He, Z.Z., Sun, Z.Q., Liu, J. (2012). A new nano-cryosurgical modality for tumor treatment using biodegradable MgO nanoparticles. Nanomedicine: Nanotechnology, Biology and Medicine, 8(8): 1233-1241. https://doi.org/10.1016/j.nano.2012.02.010

[15] Tabrez, S., Khan, A.U., Hoque, M., Suhail, M., Khan, M.I., Zughaibi, T.A. (2022). Investigating the anticancer efficacy of biogenic synthesized MgONPs: An in vitro analysis. Frontiers in Chemistry, 10: 970193. https://doi.org/10.3389/fchem.2022.970193

[16] Mahmoud, A., Ezgi, Ö., Merve, A., Özhan, G. (2016). In vitro toxicological assessment of magnesium oxide nanoparticle exposure in several mammalian cell types. International Journal of Toxicology, 35(4): 429-437. https://doi.org/10.1177/1091581816648624

[17] Rempel, S., Ogliari, A.J., Bonfim, E., Duarte, G.W., Riella, H.G., Silva, L.L., Mello, J.M.M., Baretta, C.R.D.M., Fiori, M.A. (2020). Toxicity effects of magnesium oxide nanoparticles: A brief report. Matéria (Rio de Janeiro), 25(4): e-12870. https://doi.org/10.1590/s1517-707620200004.1170

[18] Mohammed, R.S., Sudhakaran, A., Mostafa, M.Y.A., Abbady, G. (2024). Synthesize of ZnO and CuO nanoparticles with plasma jet at different treatment times and testing its optical parameters with UV-Vis-NIR. Applied Physics A, 130(8): 533. https://doi.org/10.1007/s00339-024-07651-z

[19] Saied, E., Eid, A., Hassan, S., Salem, S., Radwan, A., Halawa, M., Saleh, F., Saad, H., Saied, E., Fouda, A. (2021). The catalytic activity of biosynthesized magnesium oxide nanoparticles (MgO-NPs) for inhibiting the growth of pathogenic microbes, tanning effluent treatment, and chromium ion removal. Catalysts, 11(7): 821. https://doi.org/10.3390/catal11070821

[20] Fadhil, F.A., Taha, J.M., Khashan, K.S., Mahdi, F. (2021). Optical properties of MgO NPs produced by laser ablation in liquid. AIP Conference Proceedings, 2372(1): 080001. https://doi.org/10.1063/5.0066203

[21] Kandiah, K., Jeevanantham, T., Ramasamy, B. (2019). Reliability of antioxidant potential and in vivo compatibility with extremophilic actinobacterial-mediated magnesium oxide nanoparticle synthesis. Artificial Cells, Nanomedicine, and Biotechnology, 47(1): 862-872. https://doi.org/10.1080/21691401.2019.1580287

[22] Ali, S., Sudha, K.G., Thirumalaivasan, N., Ahamed, M., Pandiaraj, S., Rajeswari, V.D., Vinayagam, Y., Thiruvengadam, M., Govindasamy, R. (2023). Green synthesis of magnesium oxide nanoparticles by using abrus precatorius bark extract and their photocatalytic, antioxidant, antibacterial, and cytotoxicity activities. Bioengineering, 10(3): 302. https://doi.org/10.3390/bioengineering10030302

[23] Akshaykranth, A., Jayarambabu, N., Tumu, V.R., Rajaboina, R.K. (2021). Comparative study on antibacterial activity of MgO nanoparticles synthesized from Lawsonia inermis leaves extract and chemical methods. Journal of Inorganic and Organometallic Polymers and Materials, 31(6): 2393-2400. https://doi.org/10.1007/s10904-021-01915-4

[24] Nyabadza, A., Vázquez, M., Coyle, S., Fitzpatrick, B., Brabazon, D. (2021). Magnesium nanoparticle synthesis from powders via pulsed laser ablation in liquid for nanocolloid production. Applied Sciences, 11(22): 10974. https://doi.org/10.3390/app112210974

[25] Mangalampalli, B., Dumala, N., Grover, P. (2017). Acute

oral toxicity study of magnesium oxide nanoparticles and microparticles in female albino Wistar rats. Regulatory Toxicology and Pharmacology, 90: 170-184. https://doi.org/10.1016/j.yrtph.2017.09.005

[26] Hussain, R., Naz, S., Alam, S., Ali, H.M., Ali, A., Khan, M.S., Fouad, D., Ataya, F.S., Mammadov, A., Li, K. (2025). Temporal and dosage impact of magnesium oxide nanoparticles on grass carp: Unveiling oxidative stress, DNA damage, and antioxidant suppression. Toxicology Mechanisms and Methods, 35(1): 19-31. https://doi.org/10.1080/15376516.2024.2382801

[27] Shafiq, A.A., Luaib, N.M., Mahdi, R.H., Alsaimary, I.E. (2024). Oral toxicity of magnesium oxide nanoparticles, MgO NPs on liver in male rats. Iraqi Journal of Science, 65(11): 6323-6335. https://doi.org/10.24996/ijs.2024.65.11.11

[28] Majeed, S.I., Mohammed, S.M., Mohammad, A.M. (2023). Bioaccumulation and evaluation of magnesium oxide nanoparticles toxicity and combination effects of vitamin E and C with it on exposed male rats. Kurdistan Journal of Applied Research, 8(1): 1-10. https://doi.org/10.24017/Science.2023.1.1

[29] Abdulkhaleq, N.A., Nayef, U.M., Albarazanchi, A.K.H. (2020). MgO nanoparticles synthesis via laser ablation stationed on porous silicon for photoconversion application. Optik, 212: 164793. https://doi.org/10.1016/j.ijleo.2020.164793

[30] National Research Council. (2011). Guide for the Care and Use of Laboratory Animals, Eighth Edition. Washington, D.C.: The National Academies Press. https://doi.org/10.17226/12910

[31] GraphPad Prism (Version 10). La Jolla, CA, USA: GraphPad Software Inc. https://www.graphpad.com.

[32] Holzwarth, U., Gibson, N. (2011). The Scherrer equation versus the "Debye-Scherrer equation." Nature Nanotechnology, 6(9): 534. https://doi.org/10.1038/nnano.2011.145

[33] Tauc, J., Grigorovici, R., Vancu, A. (1966). Optical properties and electronic structure of amorphous germanium. Physica Status Solidi B, 15(2): 627-637. https://doi.org/10.1002/pssb.19660150224

[34] Bindhu, M.R., Umadevi, M., Kavin Micheal, M., Arasu, M.V., Abdullah Al-Dhabi, N. (2016). Structural, morphological and optical properties of MgO nanoparticles for antibacterial applications. Materials Letters, 166: 19-22. https://doi.org/10.1016/j.matlet.2015.12.020

[35] Rueden, C.T., Schindelin, J., Hiner, M.C., DeZonia, B.E., Walter, A.E., Arena, E.T., Eliceiri, K.W. (2017). ImageJ2: ImageJ for the next generation of scientific image data. BMC Bioinformatics, 18(1): 529. https://doi.org/10.1186/s12859-017-1934-z

[36] Ahmed, R.S., Mohammed, R.S., Abdul Majeed, A.M., Sudhakaran, A. (2024). Biological activity of MgO nanoparticle synthesis by plasma-assisted reduction method. Physica Scripta, 99(11): 115901. https://doi.org/10.1088/1402-4896/ad7dbc

[37] Williams, D.B., Carter, C.B. (2009). Transmission Electron Microscopy. Boston, MA: Springer US. https://doi.org/10.1007/978-0-387-76501-3

[38] Ghorbani, S., Moshtaghi, H., Shekarforoush, S.S., Gheisari, H.R., Sedaghati, F., Nazifi, S., Ahmadi, N. (2023). Histopathologic, biochemical, and biodistribution studies of orally administrated silica and magnesium oxide nanoparticles in rats. Iranian Journal of Science, 47(3): 695-705. https://doi.org/10.1007/s40995-023-01451-5

[39] Mohammed, R.S., Aadim, K.A., Ahmed, K.A. (2023). Histological, haematological, and thyroid hormones toxicity of female rats orally exposed to CuO/ZnO core/shell nanoparticles synthesized by Ar plasma jets. Archives of Toxicology, 97(4): 1017-1031. https://doi.org/10.1007/s00204-023-03462-y

[40] Parasuraman, S. (2011). Toxicological screening. Journal of Pharmacology and Pharmacotherapeutics, 2(2): 74-79. https://doi.org/10.4103/0976-500X.81895

[41] Mazaheri, N., Naghsh, N., Karimi, A., Salavati, H. (2019). In vivo toxicity investigation of magnesium oxide nanoparticles in rat for environmental and biomedical applications. Iranian Journal of Biotechnology, 17(1): 1-9. https://doi.org/10.21859/ijb.1543

[42] Kiranmai, G., Reddy, A.R.N. (2013). Antioxidant status in MgO nanoparticle-exposed rats. Toxicology and Industrial Health, 29(10): 897-903. https://doi.org/10.1177/0748233712446723

[43] Mangalampalli, B., Dumala, N., Perumalla Venkata, R., Grover, P. (2018). Genotoxicity, biochemical, and biodistribution studies of magnesium oxide nano and microparticles in albino Wistar rats after 28-day repeated oral exposure. Environmental Toxicology, 33(4): 396-410. https://doi.org/10.1002/tox.22526